Nanoscale Research Letters

NANO EXPRESS

Open Access

Biocompatible $FePO_4$ Nanoparticles: Drug Delivery, RNA Stabilization, and Functional Activity

Sagar Rayamajhi[1,2†], Sarah Wilson[2†], Santosh Aryal[3*] and Robert DeLong[2*]

Abstract

$FePO_4$ NPs are of special interest in food fortification and biomedical imaging because of their biocompatibility, high bioavailability, magnetic property, and superior sensory performance that do not cause adverse organoleptic effects. These characteristics are desirable in drug delivery as well. Here, we explored the $FePO_4$ nanoparticles as a delivery vehicle for the anticancer drug, doxorubicin, with an optimum drug loading of 26.81% ± 1.0%. This loading further enforces the formation of Fe^{3+} doxorubicin complex resulting in the formation of $FePO_4$-DOX nanoparticles. $FePO_4$-DOX nanoparticles showed a good size homogeneity and concentration-dependent biocompatibility, with over 70% biocompatibility up to 80 µg/mL concentration. Importantly, cytotoxicity analysis showed that Fe^{3+} complexation with DOX in $FePO_4$-DOX NPs enhanced the cytotoxicity by around 10 times than free DOX and improved the selectivity toward cancer cells. Furthermore, $FePO_4$ NPs temperature-stabilize RNA and support mRNA translation activity showing promises for RNA stabilizing agents. The results show the biocompatibility of iron-based inorganic nanoparticles, their drug and RNA loading, stabilization, and delivery activity with potential ramifications for food fortification and drug/RNA delivery.

Keywords: Iron phosphate nanoparticles, Doxorubicin, Drug delivery, Drug loading, RNA stabilization, Biocompatible nanoparticles

Introduction

Among various inorganic nanoparticles such as gold, silica, and quantum dots, iron-based nanoparticles (Fe-NPs) are widely explored for biomedical applications like contrast agents, drug delivery vehicles, and thermal-based therapeutics [1–3]. Owing to the magnetic property, high bio-adaptability, and known endogenous metabolism of iron, Fe-NPs are desirable candidates for biomedical applications. As such, Fe-NPs make the majority of FDA-approved inorganic nanomedicine [1, 2]. These include INFeD, DexFerrum, Ferrlecit, Venofer, Feraheme, and Injectafer which are commercially available for their application in iron-deficient anemia and iron deficiency in chronic kidney disease [1]. Similarly, intravenous administration of the chelate iron gluconate is a well-tolerated intervention for anemia [4]. Anemia is one of the most prevalent nutritional deficiency in the world and Fe-based nanoparticles like $FePO_4$ and $FeSO_4$ has been used in food fortification to prevent anemia. Food fortification is the process of adding micronutrients to the food with an aim to overcome the nutritional deficiency in a population [5]. $FePO_4$ NPs are of special interest in food fortification because of their biocompatibility, high bioavailability, and superior sensory performance that do not cause adverse organoleptic effects [6–9]. Perfecto et al. have demonstrated the $FePO_4$ NPs

*Correspondence: santosharyal@uttyler.edu; robertdelong@ksu.edu
†Sagar Rayamajhi and Sarah Wilson have contributed equally to this work
[2] Nanotechnology Innovation Center of Kansas State, College of Veterinary Medicine, Kansas State University, Manhattan, KS 66502, USA
[3] Department of Pharmaceutical Sciences and Health Outcomes, The Ben and Maytee Fisch College of Pharmacy, The University of Texas at Tyler, Tyler, TX 75799, USA
Full list of author information is available at the end of the article

internalization in human intestinal cells occurs primarily through divalent metal transporter-1 (DMT-1) and therefore can be readily absorbed [9, 10]. Iron-based Feridex® and Revosit® are widely used magnetic resonance imaging (MRI) contrast agents for contrast enhanced MRI [11–16]. In light of these outstanding reports, $FePO_4$ NPs present themselves as a good delivery vehicle. Here, we explored $FePO_4$ as a drug-delivery vehicle by loading an anticancer drug, Doxorubicin (DOX). Ferric ion (Fe^{3+}) can form complex with DOX molecule facilitated by electrostatic interaction between electron deficient Fe in $FePO_4$ and electron rich –OH group in DOX to form DOX loaded $FePO_4$ NPs: $FePO_4$-DOX NPs. We evaluated the physicochemical properties of $FePO_4$ and $FePO_4$-DOX NPs and assessed their biocompatibility and cytotoxicity profile, respectively, in mouse osteosarcoma K7M2 and fibroblast NIH/3T3 cell-line.

Along with that, the inorganic nanoparticle has shown promises in nucleic acid stabilization and delivery [17–19]. In this regard, the gold nanoparticle has been widely studied because of their ability to immobilize oligonucleotides in their surface resulting in the prevention of molecular aggregation and degradation [17, 20]. However, gold is not an endogenous element and thereby may limit its translational application. Here, Fe-based nanoparticles like $FePO_4$ nanoparticles can be of prime interest for RNA stabilization study because of their endogenous nature and established biocompatibility profile. There is two proposed mechanism of interaction of nucleic acid (RNA/DNA) with Fe-NPs for the stabilization—(1) formation of hydrogen bonds and electrostatic interaction between the phosphate group of nucleic acid backbone and Fe-NPs resulting in adsorption of nucleic acid in Fe-NPs, and (2) nucleic acid can adsorb to the Fe-NPs surface via nucleotide base pair interaction [19, 21, 22]. A study has shown the potential of calcium phosphate nanoparticles for DNA vaccine stabilization and delivery [23]. In this regard, here we have explored the RNA stabilization and functional activity of another phosphate-based nanoparticle, $FePO_4$, to investigate the multifunctional potential of $FePO_4$ based nanoparticles, in the delivery and stabilization of cargo.

With rapid approval of mRNA vaccine against COVID19, mRNA vaccine nanoparticles are of great interest, RNA being subject to rapid hydrolysis and loss of functional expression, it is incumbent upon the nanoparticle to improve these critical characteristics. Here we show $FePO_4$ NPs stabilize RNA and support functional mRNA translation. Given these excellent characteristics, $FePO_4$ NPs may merit consideration for food fortification, drug, and RNA delivery, opening up exciting biomedical applications.

Results and Discussion

$FePO_4$ NPs Synthesis, Characterization, and Biocompatibility Analysis

A simple one-step chemical reaction between $(NH_4)_3PO_4$ and $Fe(NO_3)_3$ gives $FePO_4$ as precipitate which is dispersed in biocompatible lipid-PEG surfactant that helps to stabilize $FePO_4$ nanoparticles and prevent aggregation. $FePO_4$ NPs showed a hydrodynamic size of 175 ± 5 nm with a polydispersity index (PDI) of 0.150 ± 0.01 suggesting good particle homogeneity and narrow size distribution. Zeta potential analysis showed a negative surface charge of $FePO_4$ NPs with -19.1 ± 8 mV zeta potential. The negative surface charge further helps to stabilize particles in colloids thereby preventing protein opsonization, a mechanism that prevents cellular targeting and alters pharmacokinetics [24–26]. $FePO_4$ was further characterized by FTIR. Figure 1c shows the spectral characteristic of $FePO_4$ nanoparticles and their precursor—$Fe(NO_3)_3$ and $(NH_4)_3PO_4$. $FePO_4$ spectra show a distinct sharp peak on 1030 cm^{-1} which can be attributed to the P–O stretching band, a small peak at 520 cm^{-1} corresponds to the O–P–O antisymmetric bending, and a broad ranges from 3000 to3500 cm^{-1} represents water bending and stretching vibrations from adsorbed water molecules [27, 28]. The $FePO_4$ spectra showed the presence of PO_4^{3-} group and are similar to the FTIR peak reported by other studies thus confirming the formation of $FePO_4$ nanoparticles [27–29]. $Fe(NO_3)_3$ spectra showed characteristic peaks for N–O stretching bands at 1326 and 813 cm^{-1} [30]. Peak at 1625 can be attributed to –OH bending vibration and a broad peak around 3000 cm^{-1} can be attributed to water bending and stretching vibrations [30]. Likewise, $(NH_4)_3PO_4$ showed characteristic peaks for the ammonium group around 1500 cm^{-1} and phosphate group around 1000 cm^{-1} [31]. The absence of nitrate and ammonium peaks in $FePO_4$ nanoparticles suggest the product is free from possible byproducts and confirms the purity of synthesis.

With the assurance of successful synthesis, purity, good size homogeneity, and stable surface charge of $FePO_4$ NPs, we went on to analyze the biocompatibility of $FePO_4$ NPs. For this purpose, we used cancer and non-cancer cells: mouse osteosarcoma K7M2 and mouse fibroblast NIH/3T3 and analyzed the biocompatibility of NPs at a varying concentration in terms of cell viability using MTT assay. $FePO_4$ NPs showed concentration-dependent biocompatibility in both cell lines-K7M2 and NIH/3T3, in the concentration range of 20 to 600 µg/mL (Fig. 1d). $FePO_4$ NPs showed good biocompatibility up to 80 µg/mL concentration with cell viability greater than 70%. Biocompatibility was relatively higher in non-cancer cell NIH/3T3 compared to cancer cell K7M2.

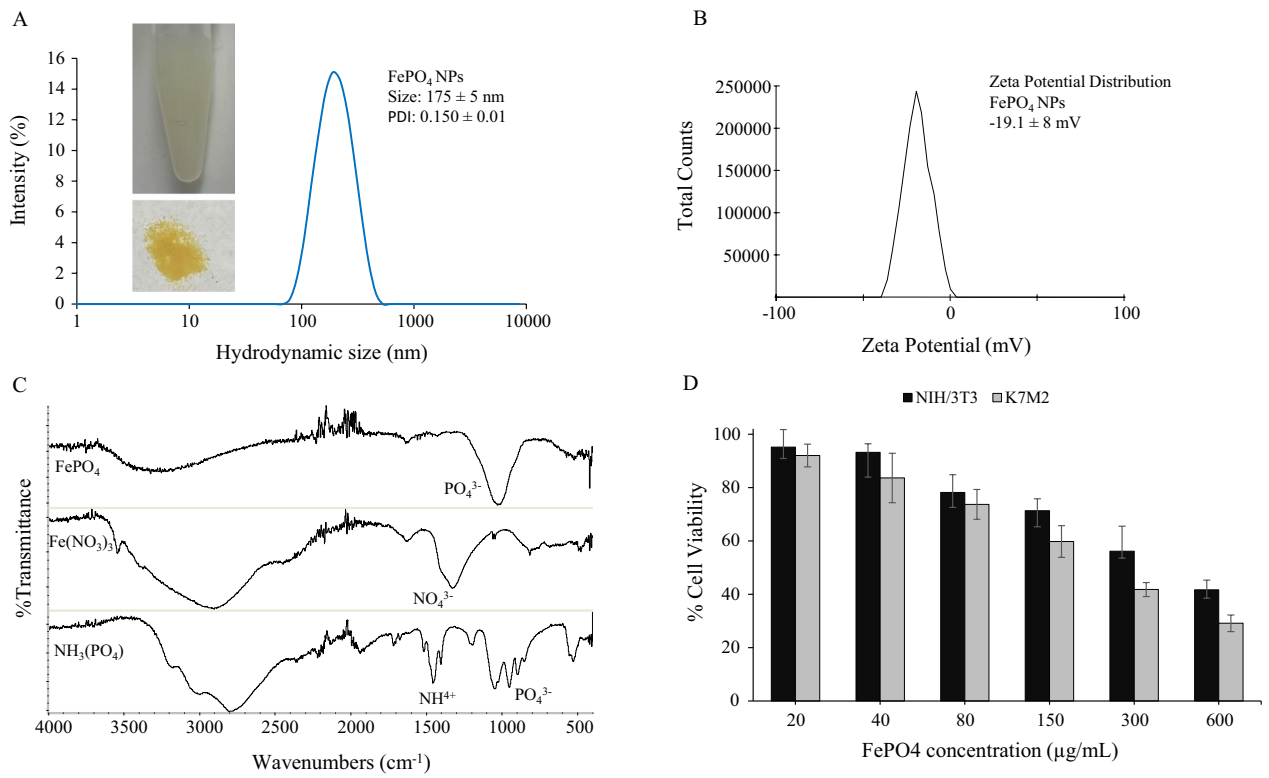

Fig. 1 Characterization and biocompatibility of $FePO_4$ nanoparticles. **a** Hydrodynamic size distribution of $FePO_4$ NPs, **b** zeta potential measurement of $FePO_4$ NPs showing the surface charge, **c** FTIR of $FePO_4$ NPs and its precursor-$Fe(NO_3)_3$ and $(NH_4)_3PO_4$, and **d** biocompatibility of $FePO_4$ NPs on mouse osteosarcoma K7M2 and mouse fibroblast NIH/3T3 cell line. NPs were treated at various concentrations for 48 h (**a, b** data represents mean ± s.d.; $n = 3$ replicates. **d** represents mean ± s.d., $n = 6$ replicates).

Doxorubicin Loading in $FePO_4$ and Cytotoxicity of $FePO_4$-DOX

Doxorubicin is loaded in $FePO_4$ through the co-incubation-precipitation method in which doxorubicin solution is mixed with the precursor of $FePO_4$ that results in the formation of DOX loaded $FePO_4$. Three different formulations to load DOX are employed as discussed in the methods. Formulation 1 showed the best loading efficiency of 26.81% ± 1 whereas formulation 2 showed a loading efficiency of 8.83% ± 2 and formulation 3 did not show any loading (Fig. 2a). For loading, we added DOX solution to the precursor $Fe(NO_3)_3$ in formulation 1 and to $(NH_4)_3PO_4$ in formulation 2, whereas, in formulation 3, we added DOX solution to $FePO_4$ NPs directly. The loading data clearly showed that adding DOX to the $FePO_4$ NPs does not retain the DOX whereas adding DOX to either precursor: $Fe(NO_3)_3$ and $(NH_4)_3PO_4$ solution helps in the loading and retention of DOX. This can be explained by the fact that Fe^{3+} from $Fe(NO_3)_3$ can form a complex with the electron-rich oxygen group present in Doxorubicin [32, 33]. The Fe^{3+}-DOX complex is then precipitated by the addition of $(NH_4)_3PO_4$ resulting in $FePO_4$-DOX, which is characterized by a change of color from faint yellow to faint brown (Fig. 2b). Despite the color change, there was no change in the emission spectra of $FePO_4$-DOX which showed emission maxima at 590 nm similar to that of Free DOX, when excited at 480 nm (Fig. 2c). $FePO_4$-DOX NPs showed a hydrodynamic size of 187 ± 7 nm and PDI of 0.143 ± 0.02, similar to that of $FePO_4$ (Fig. 2d). However, there was a significant difference in the surface charge of $FePO_4$-DOX NPs (-8.89 ± 5 mV), compared to $FePO_4$ NP (-19.1 ± 8 mV) (Fig. 2e). Change in zeta potential suggests functional changes in the surface property of nanoparticles. Here, the reduction of zeta potential from −19.1 to −8.89 mV can be attributed to the DOX complexation which adds cationic property in the complex.

Following the physicochemical characterization, the cytotoxicity of $FePO_4$-DOX was analyzed in K7M2 and NIH/3T3 cells and compared with free DOX (Fig. 3). $FePO_4$-DOX showed higher cytotoxicity compared to Free DOX at equivalent DOX concentration in both cell lines. IC50 value showed around 10 times reduction with $FePO_4$-DOX treatment, from 2.61 to 0.248 µM in NIH/3T3 and 1.01 to 0.107 µM in K7M2 cells. This drastic reduction in IC50 value in both cell lines suggests

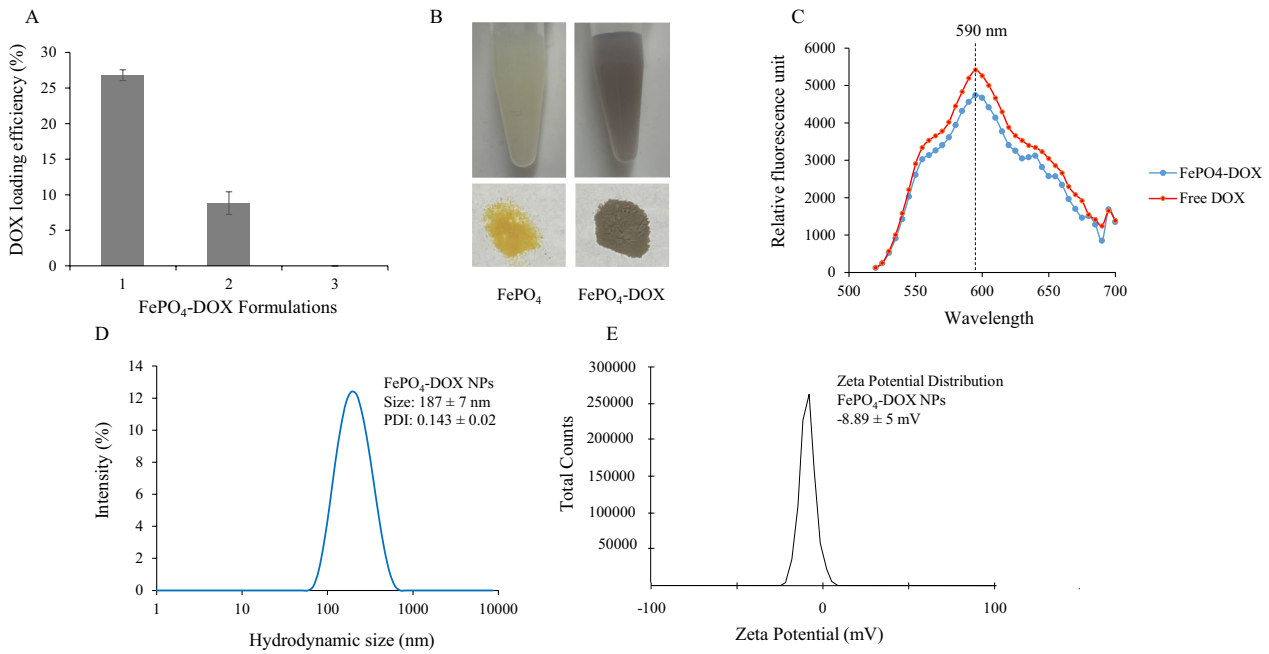

Fig. 2 Doxorubicin (DOX) loading in $FePO_4$ NPs and characterization of $FePO_4$-DOX. **a** DOX loading efficiency in three different formulations of $FePO_4$ NPs and DOX, **b** pictorial representation of the change of color from yellow to brown after DOX loading in $FePO_4$ to formulate $FePO_4$-DOX, **c** emission spectra characterization of DOX loaded $FePO_4$ NPs ($FePO_4$-DOX) after excitation at 480 nm, **d** hydrodynamic size distribution of $FePO_4$-DOX NPs, and **e** zeta potential characterization of $FePO_4$-DOX NPs showing surface charge (data represents mean ± s.d.; $n = 3$ replicates)

an enhanced cytotoxicity profile of $FePO_4$-DOX NPs. The equivalent $FePO_4$ concentration in the IC50 concentration range of $FePO_4$-DOX is 40 μg/mL (0.107 μM in K7M2 cells) and 100 μg/mL (0.248 μM in NIH/3T3 cells), which are both within the biocompatible range of $FePO_4$ concentration, with more than 70% cell viability. Hence, the elevation of $FePO_4$-DOX cytotoxicity can be attributed to the Fe^{3+}-DOX complex formation and not to the individual contribution of $FePO_4$ and DOX. Literature has shown the elevated cytotoxic effect of anthracycline like doxorubicin in presence of iron [34–37]. These reports are further supported by the alleviation of Fe-DOX cytotoxicity by the use of iron chelators [35–37]. One proposed mechanism is Fe-DOX complex potentiates the toxicity of DOX-derived reactive oxygen species (ROS) transforming relatively safe ROS ($O^{2\cdot}-$ and H_2O_2) into much more toxic ROS leading to elevated DNA damage and cell death [34, 36]. Another proposed mechanism is the interaction of DOX with the function of iron regulatory proteins and ferritin in presence of excess Fe thereby affecting iron homeostasis leading to ROS-dependent and independent damage and apoptotic cell death [36, 38].

Along with the elevated cytotoxicity, $FePO_4$-DOX showed selectivity toward cancer cells with higher cytotoxicity behavior similar to that of Free DOX. Figure 3c shows 0.1 μM DOX equivalent $FePO_4$-DOX showed 53% cell viability for cancer cell K7M2 compared to 72% cell viability for non-cancer NIH/3T3. Likewise, Free DOX also showed higher cytotoxicity behavior toward cancer cells, with 54% cell viability in K7M2 cells compared to 66% in NIH/3T3. However, the differences have increased in the case of $FePO_4$-DOX, with 19% differences in cell viability among cancer and non-cancer cells compared to 12% in Free DOX. Cytotoxicity analysis has shown that Fe complexation with DOX in $FePO_4$-DOX NPs has significantly enhanced the cytotoxicity and improved the selectivity toward cancer cells.

Cellular Internalization of $FePO_4$-DOX NPs

The internalization behavior of $FePO_4$-DOX NPs was analyzed using confocal microscopy following a time-dependent internalization study (Fig. 4). Free DOX was used as a positive control. Both $FePO_4$-DOX NPs and Free DOX did not show significant internalization in the initial 0.5 and 1 h incubation time points. However, at 3 h incubation, both showed internalization as depicted by red DOX fluorescence in the confocal image. The blue color comes from nucleus staining by DAPI. The analysis shows that within 3 h, $FePO_4$-DOX NPs internalize to cells following similar internalization behavior as that of Free DOX. It is important to note that, due

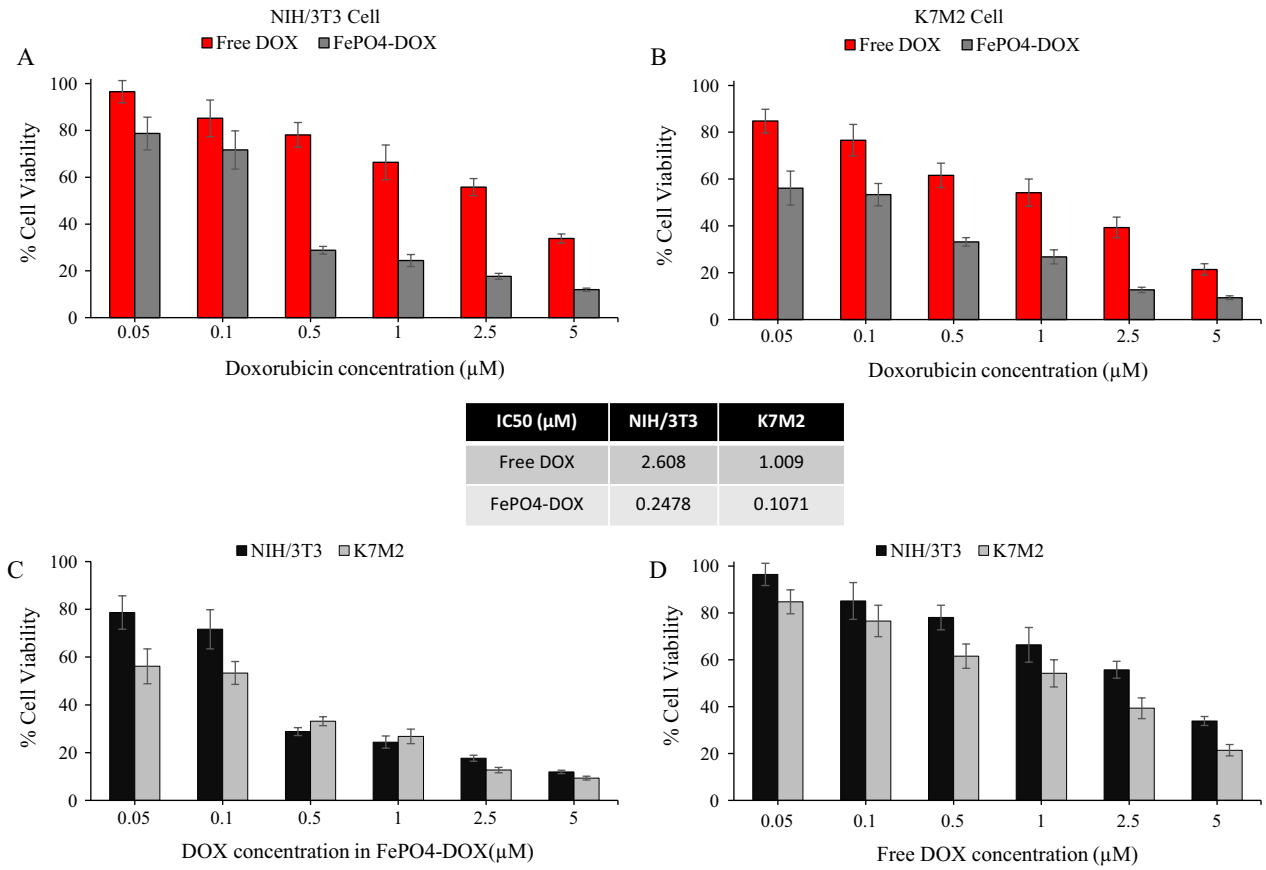

IC50 (μM)	NIH/3T3	K7M2
Free DOX	2.608	1.009
FePO4-DOX	0.2478	0.1071

Fig. 3 Cytotoxicity of $FePO_4$-DOX NPs. **a, b** Cytotoxicity of Free Doxorubicin (DOX) and $FePO_4$-DOX NPs in mouse fibroblast NIH/3T3 and osteosarcoma K7M2 cell-line, respectively, at various DOX equivalent concentration. Cytotoxicity was analyzed in percentage cell viability after particle treatment for 48 h. **c, d** A comparison in percentage cell viability of $FePO_4$-DOX NPs and Free DOX in NIH/3T3 and K7M2 cell lines, respectively, at equivalent DOX concentration. The inset in the middle represents the IC-50 values of Free DOX and $FePO_4$-DOX NPs in NIH/3T3 and K7M2 cells (data represents mean ± s.d.; $n = 6$ replicates)

to the change of color of $FePO_4$-DOX, which is brownish compared to the red color of Free DOX, we may not quantitatively compare the relative internalization profile of $FePO_4$-DOX. Nonetheless, the internalization assay confirmed that $FePO_4$-DOX is uptake by the cells within 3 h. Given the well-understood mechanism of handling iron by our body, proposed NPs could hold promises in the development of iron-based anticancer therapeutics with an ability to monitor therapeutic response in a single therapy session.

RNA Stabilization and mRNA Expression

As can be seen in Fig. 5a, whereas copper nanoparticles (Cu NP) and carbon nanotubes (CNTs) accelerate RNA hydrolytic degradation (lower band intensity than control), the $FePO_4$ and control silver (Ag) nanoparticle stabilize the RNA as shown by relatively strong band intensity in RNA agarose gel electrophoresis (RAGE). The $FePO_4$ and control zinc oxide nanoparticle (ZnO NP) also impart some resistance to degradation in serum, as depicted by the band intensity which is slightly higher than controls (Fig. 5b). Importantly the functional activity, mRNA expression is higher than non-nanoparticle controls, whereas the RNA-degrading Cu NP causes loss in mRNA expression as measure by relative light units (Fig. 5c). These results show that $FePO_4$ NPs helps to stabilize RNA and can be used as a stabilizing delivery agent for therapeutic RNA delivery. Earlier preliminary experiments had indicated a normal working range of translation shown are two independent experiments for the control non-nanoparticle treated samples showing 2393 and 2630 RLU/well which is representative. A twofold increase consistent with the above data suggests FePO44 NP supports translation whereas consistent with RNA denaturation/degradation above, the Cu NP suppresses translation. A variety of inorganic nanoparticle systems have been exploited for therapeutic RNA stabilization and delivery including; gold, silver, copper, iron oxide,

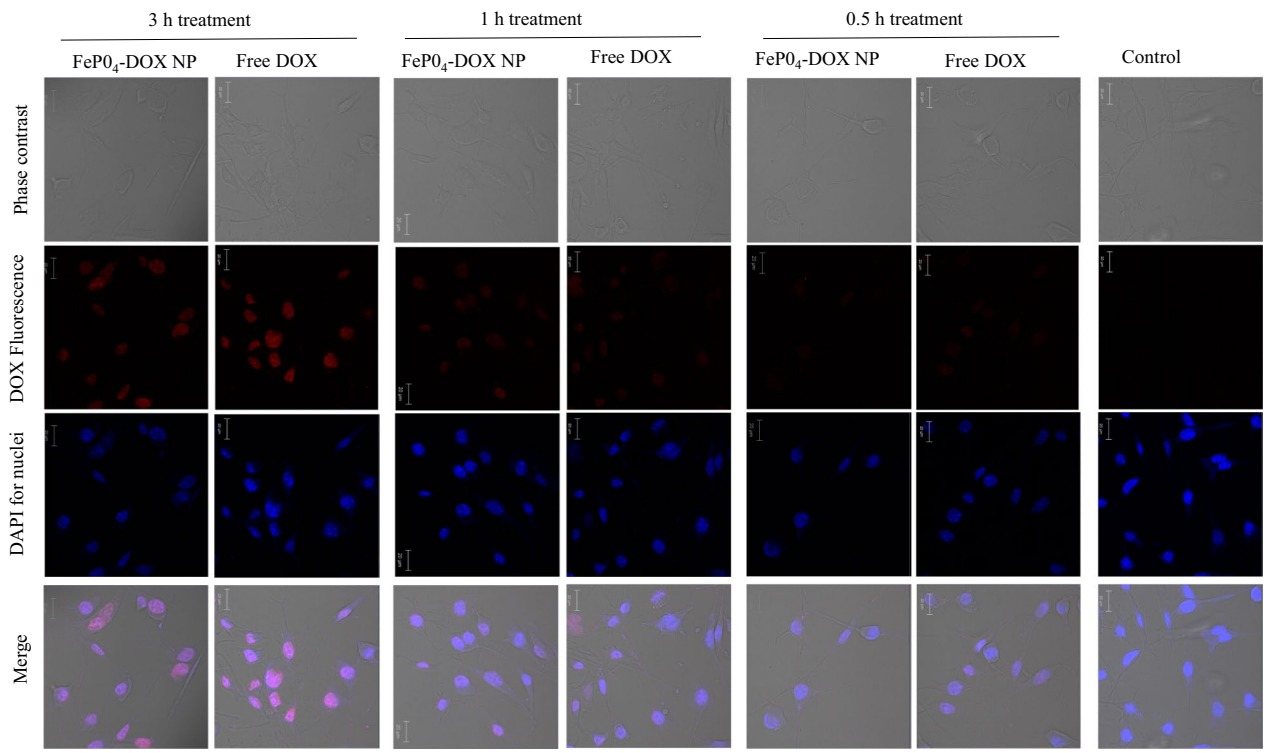

Fig. 4 Cellular internalization study. Cellular internalization of $FePO_4$-DOX NPs and Free DOX on K7M2 cells after 3 h, 1 h, and 0.5 h treatment. Cells were treated with 200 µL of 5 µg/mL DOX concentration. The red color observed in nanoparticle treated cell line signify successful internalization of the nanoparticles. The red color is due to the fluorescence characteristic of DOX. No red signal is observed in the untreated control cell

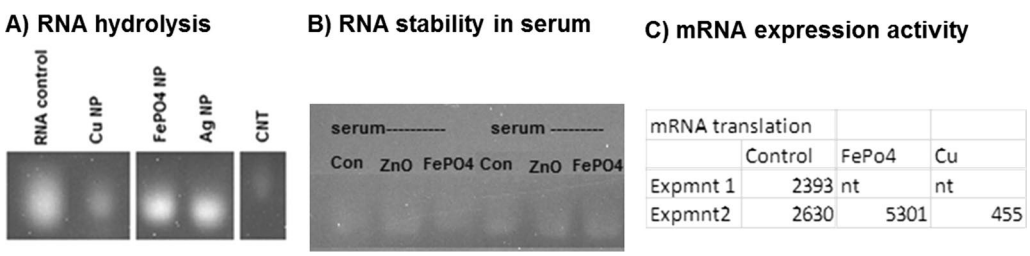

Fig. 5 RNA hydrolysis. **a** A model RNA we have used in a number of our publications similar in size and sequence composition to most mRNAs from torula yeast (TY-RNA) was used. The RNA was incubated in double-distilled water over time in the presence or absence of nanoparticles either copper (Cu NP), iron phosphate (FePO4), silver (Ag NP) or carbon nanotube (CNT) at 37 degrees celcius and samples removed at the same time point and assayed by RNA agarose gel electrophoresis (RAGE). Loss of band staining intensity indicates RNA degradation whereas maintenance of RNA band staining intensity indicates stabilization. **b** Similar to above, RNA was incubated in 10% FBS/DMEM at room temperature in the presence of zinc oxide (ZnO) NP or $FePO_4$ NP versus control which was RNA alone in the absence of nanoparticle. Again samples were removed over time and assayed by RAGE, presence of the stained RNA band over time again indicates stability and resistance from nuclease or RNase degradation from the serum. **c** mRNA encoding Luciferase was translated in vitro from standard rabbit reticulocyte and the relative luminescence standardized to RNA in the presence or absence of either iron phosphate ($FePO_4$) or copper (Cu) nanoparticle

mesoporous silica nanoparticle (MSN), carbon-based polymers, composites, and others [39–45]. For example our group had reported nanoparticle complexation to macromolecular RNA can cause it to resist degradation by RNase, or nucleases present in serum and tissues. The COVID-19 mRNA vaccine has renewed interest in such macromolecular RNA therapies extending beyond vaccines, where it is incumbent upon the nanoparticle to not only protect RNA from hydrolysis and nuclease-mediated digestion, but complexation to the NP must preserve RNA function, for example, mRNA expression. Previously we had seen copper nanoparticle complexation macromolecular RNA causes RNA denaturation [46] Thus we investigated the effects of NP complexation to

macromolecular RNA using Torula yeast RNA (TY-RNA) or a reporter construct mRNA expressing Luciferase.

Conclusion

$FePO_4$ nanoparticles were successfully synthesized following a simple co-incubation-precipitation technique resulting in the formation of homogenous-sized particles of 175 ± 5 nm. FTIR analysis confirmed the presence of phosphate group and the absence of precursor impurities in the nanoparticle. Biocompatibility analysis revealed concentration-dependent biocompatibility with more than 70% cell viability up to 80 μg/mL. Further, DOX was effectively loaded in $FePO_4$ resulting in $FePO_4$-DOX NPs which showed similar physicochemical properties to that of $FePO_4$. Cytotoxicity analysis revealed that Fe complexation with DOX in $FePO_4$-DOX NPs enhanced the cytotoxicity, with around 10 times improvement in IC50, and improved the selectivity toward cancer cells. Additionally, the internalization assay showed $FePO_4$-DOX NPs were efficiently internalized in cells at a 3 h incubation time point. RNA stabilization study showed that $FePO_4$ nanoparticles efficiently stabilize RNA, prevent rapid degradation, and maintain the functional activity demonstrating promises for delivery of therapeutic RNA. Given the good size homogeneity, biocompatibility range, drug loading efficiency, enhanced cytotoxicity profile, RNA stabilizing property, and efficient cellular uptake, $FePO_4$ NPs showed desirable characteristics for drug and RNA delivery vehicles. Furthermore, the results have shown promising prospects of using $FePO_4$-drug NPs in food fortifications for the development of a food-based drug platform.

Methods

Synthesis and Characterization of $FePO_4$ Nanoparticles

$FePO_4$ nanoparticles were synthesized by chemical precipitation technique optimizing protocol by Sokolova et al. [47]. Briefly, Ammonium phosphate ($(NH_4)_3PO_4$, 16 mg/mL) and iron nitrate ($Fe(NO_3)_3$, 8 mg/mL) solution was prepared. To the 1 mL of $Fe(NO_3)_3$, 1 mL of $(NH_4)_3PO_4$ was added dropwise under constant stirring resulting in precipitation of iron phosphates ($FePO_4$). Excess of $(NH_4)_3PO_4$ was used so that all Fe from $Fe(NO_3)_3$ precipitate as $FePO_4$. Thus formed iron phosphates solution was washed with water 3 times to remove byproducts by centrifuging at 300 g for 2 min. Finally, $FePO_4$ precipitate was dispersed with DSPE-PEG-COOH solution (10% w/w) in water to formulate $FePO_4$ nanoparticles. $FePO_4$ NPs were characterized for size and surface property using dynamic light scattering (DLS) and spectral characteristics using Fourier Transform Infrared Spectroscopy (FTIR).

Doxorubicin (DOX) Loading on $FePO_4$ Nanoparticles

Doxorubicin was loaded in $FePO_4$ nanoparticles by the co-incubation-precipitation method. Three different DOX-$FePO_4$ NPs formulations were explored to optimize the best loading efficiency. In the first formulation, DOX-$FePO_4$ NPs were formulated by adding 100 μg DOX in 1 mL of $Fe(NO_3)_3$ (8 mg/mL) followed by the addition of 1 mL of $(NH_4)_3PO_4$ (16 mg/mL) dropwise under constant stirring. In the second formulations, 100 μg DOX was first added to 1 mL of $(NH_4)_3PO_4$ (16 mg/mL) followed by the addition of 1 mL of $Fe(NO_3)_3$ (8 mg/mL) dropwise under constant stirring. In the third formulations, 100 μg DOX was added to the $FePO_4$ NP solution. Thus formulated $FePO_4$-DOX NPs were washed three times with water and the amount of doxorubicin in $FePO_4$-DOX was quantified spectrofluorimetrically by measuring DOX excitation and emission at 490 nm and 595 nm.

DOX loading efficiency was calculated by the following equation:

$$\%\ \text{Loading efficiency: (DOX present in } FePO_4 - \text{DOX NP/Initial input of DOX)} \times 100$$

Biocompatibility of $FePO_4$ NPs and Cytotoxicity of $FePO_4$-DOX NPs

Biocompatibility of $FePO_4$ NPs and cytotoxicity of $FePO_4$-DOX NPs were assayed in mouse osteosarcoma K7M2 and mouse fibroblast NIH/3T3 using MTT assay following established protocol [48, 49]. Briefly, 10,000 cells were seeded in 96 well plates and incubated for 24 h in a 37 °C 5% CO_2 incubator. Then, media was removed and fresh media with varying concentrations of nanoparticles were treated to cells and left for incubation for 48 h. Control cells were maintained with media only. $FePO_4$ NPs concentration ranges from 20 to 600 μg/mL and DOX concentration ranges from 0.05 to 5 μM. After NP incubation, media was removed and cells were incubated with MTT solution (0.5 mg/ml) in serum-free media for 2 h to allow for the formation of formazan crystal. MTT solution was removed and formazan crystal was dissolved in DMSO and left for 15 min at room temperature for proper mixing. Then the absorbance of DMSO solution was measured at 550 nm using a microplate reader (BioTek, Synergy H1 Hybrid Reader) and percentage cell viability was calculated.

Cellular Internalization via Confocal Microscopy

Cellular internalization of $FePO_4$-DOX NPs was analyzed in mouse osteosarcoma K7M2 cells using confocal microscopy [49–51]. Briefly, 12,000 cells were seeded in 8-well plates and incubated for 24 h in 37 °C 5% CO_2 incubator. Then, 200 µL of 5 µg/mL DOX concentration in media were treated for 3 h, and cells were fixed with 4% Paraformaldehyde for imaging. The nucleus was stained by DAPI and cells were observed under a Confocal Laser Scanning Microscope (Carl Zeiss, LSM-700). Here, the emission maximum of DOX at 560 nm can be exploited to track its internalization which gives red color in confocal microscopy. Using the same protocol, a time-dependent internalization assay was performed by incubating $FePO_4$-DOX NPs and Free DOX for 0.5, 1, and 3 h respectively.

RNA Stability and Expression

Torula yeast RNA (Sigma-Aldrich) was dissolved at 1 mg/ml in sterile deionized water and 2 µg aliquots exposed to 20 ug/mL nanoparticle (CNT, Cu, Ag, ZnO NP or $FePO_4$) incubated at 37 deg C and assayed over time by RNA agarose gel electrophoresis as we have previously reported [42, 52]. Timepoint shown in Fig. 5 is overnight. Similarly, the RNA with/without nanoparticles was exposed to 10% FBS/DMEM and again assayed by RAGE as above. mRNA fLuc was obtained from Trilink Biotechnologies, 2 µl were incubated in rabbit reticuloysate supplemented with Methinine, Cysteine and Leucine (ProMega Corp) for 30 degrees for 1.5 h with or without nanoparticle at 20 µg/ml, standard Luciferin reagent added, and luminescence measurement taken on a Biotek Synergy H1 plate reader under standard conditions.

Statistical Analysis

All data represents at least three independent replicates and expressed as mean ± s.d. whenever possible. Cell viability data includes six replicates.

Acknowledgements

The authors acknowledge the support from National Science Foundation (NSF Award Number: 2029579).

Authors' Contributions

SA and RD conceived the study and discussed with SR and SW. SR and SW conducted all the experiment in supervision of SA and RD. SR and SA prepared the manuscript. RD finalized RNA part. SA and RD edited the final manuscript with input from all authors. All authors read and approves the final manuscript.

Availability of Data and Materials

The datasets used and/or analyzed during the current study are available from the corresponding author on reasonable request.

Declarations

Competing interests

Authors declare no conflict of interest.

Author details

[1]Department of Chemistry, Kansas State University, Manhattan, KS 66502, USA. [2]Nanotechnology Innovation Center of Kansas State, College of Veterinary Medicine, Kansas State University, Manhattan, KS 66502, USA. [3]Department of Pharmaceutical Sciences and Health Outcomes, The Ben and Maytee Fisch College of Pharmacy, The University of Texas at Tyler, Tyler, TX 75799, USA.

Received: 19 October 2021 Accepted: 11 November 2021
Published online: 27 November 2021

References

1. Mitchell MJ, Billingsley MM, Haley RM, Wechsler ME, Peppas NA, Langer R (2021) Engineering precision nanoparticles for drug delivery. Nat Rev Drug Discov 20:101–124. https://doi.org/10.1038/s41573-020-0090-8
2. Bobo D, Robinson KJ, Islam J, Thurecht KJ, Corrie SR (2016) Nanoparticle-based medicines: a review of FDA-approved materials and clinical trials to date. Pharm Res 33:2373–2387. https://doi.org/10.1007/s11095-016-1958-5
3. Nguyen VL, Cao MT, Yang Y, Yanqin C, Haibo W, Masayuki N (2013) Synthesis and characterization of Fe-based metal and oxide based nanoparticles: discoveries and research highlights of potential applications in biology and medicine. Recent Pat Nanotechnol 8:52–61
4. Auerbach M, Macdougall I (2017) The available intravenous iron formulations: History, efficacy, and toxicology. Hemodial Int 21(Suppl 1):S83–S92. https://doi.org/10.1111/hdi.12560
5. Hurrell RF (1997) Preventing iron deficiency through food fortification. Nutr Rev 55:210–222. https://doi.org/10.1111/j.1753-4887.1997.tb01608.x
6. Hilty FM, Arnold M, Hilbe M, Teleki A, Knijnenburg JTN, Ehrensperger F, Hurrell RF, Pratsinis SE, Langhans W, Zimmermann MB (2010) Iron from nanocompounds containing iron and zinc is highly bioavailable in rats without tissue accumulation. Nat Nanotechnol 5:374–380. https://doi.org/10.1038/nnano.2010.79
7. Rohner F, Ernst FO, Arnold M, Hilbe M, Biebinger R, Ehrensperger F, Pratsinis SE, Langhans W, Hurrell RF, Zimmermann MB (2007) Synthesis, characterization, and bioavailability in rats of ferric phosphate nanoparticles. J Nutr 137:614–619. https://doi.org/10.1093/jn/137.3.614
8. von Moos LM, Schneider M, Hilty FM, Hilbe M, Arnold M, Ziegler N, Mato DS, Winkler H, Tarik M, Ludwig C, Naegeli H, Langhans W, Zimmermann MB, Sturla SJ, Trantakis IA (2017) Iron phosphate nanoparticles for food fortification: Biological effects in rats and human cell lines. Nanotoxicology 11:496–506. https://doi.org/10.1080/17435390.2017.1314035
9. Perfecto A, Elgy C, Valsami-Jones E, Sharp P, Hilty F, Fairweather-Tait S (2017) Mechanisms of iron uptake from ferric phosphate nanoparticles in human intestinal caco-2 cells. Nutrients 9:359. https://doi.org/10.3390/nu9040359
10. Yanatori I, Kishi F (2019) DMT1 and iron transport. Free Radical Biol Med 133:55–63. https://doi.org/10.1016/j.freeradbiomed.2018.07.020
11. ThanhNguyen TD, Pitchaimani A, Ferrel C, Thakkar R, Aryal S (2018) Nanoconfinement-driven enhanced magnetic relaxivity of SPIONs for targeted tumor bioimaging. Nanoscale 10:284–294. https://doi.org/10.1039/C7NR07035G
12. Morana G, Cugini C, Scatto G, Zanato R, Fusaro M, Dorigo A (2013) Use of contrast agents in oncological imaging: magnetic resonance imaging. Cancer Imaging 13:350–359. https://doi.org/10.1102/1470-7330.2013.9018
13. Cervadoro A, Cho M, Key J, Cooper C, Stigliano C, Aryal S, Brazdeikis A, Leary JF, Decuzzi P (2014) Synthesis of multifunctional magnetic nanoflakes for magnetic resonance imaging, hyperthermia, and targeting. ACS Appl Mater Interfaces 6:12939–12946. https://doi.org/10.1021/am504270c
14. Rayamajhi S, Marasini R, Thanh Nguyen TD, Plattner BL, Biller D, Aryal S (2020) Strategic reconstruction of macrophage-derived extracellular vesicles as a magnetic resonance imaging contrast agent. Biomater Sci 8:2887–2904. https://doi.org/10.1039/D0BM00128G
15. Fornasiero D, Bellen JC, Baker RJ, Chatterton BE (1987) Paramagnetic complexes of manganese(II), iron(III), and gadolinium(III) as contrast agents for magnetic resonance imaging. The influence of stability constants on the biodistribution of radioactive aminopolycarboxylate complexes. Investig Radiol 22:322–327. https://doi.org/10.1097/00004424-198704000-00008

16. Bulte JWM, Kraitchman DL (2004) Iron oxide MR contrast agents for molecular and cellular imaging. NMR Biomed 17:484–499. https://doi.org/10.1002/nbm.924
17. Jiang Y, Huo S, Hardie J, Liang X-J, Rotello VM (2016) Progress and perspective of inorganic nanoparticle-based siRNA delivery systems. Expert Opin Drug Deliv 13:547–559. https://doi.org/10.1517/17425247.2016.1134486
18. Shu Y, Pi F, Sharma A, Rajabi M, Haque F, Shu D, Leggas M, Evers BM, Guo P (2014) Stable RNA nanoparticles as potential new generation drugs for cancer therapy. Adv Drug Deliv Rev 66:74–89. https://doi.org/10.1016/j.addr.2013.11.006
19. Storhoff JJ, Elghanian R, Mirkin CA, Letsinger RL (2002) Sequence-dependent stability of DNA-modified gold nanoparticles. Langmuir 18:6666–6670. https://doi.org/10.1021/la0202428
20. DeLong RK, Reynolds CM, Malcolm Y, Schaeffer A, Severs T, Wanekaya A (2010) Functionalized gold nanoparticles for the binding, stabilization, and delivery of therapeutic DNA, RNA, and other biological macromolecules. NSA 3:53–63. https://doi.org/10.2147/NSA.S8984
21. Ghaemi M, Absalan G (2014) Study on the adsorption of DNA on Fe_3O_4 nanoparticles and on ionic liquid-modified Fe_3O_4 nanoparticles. Microchim Acta 181:45–53. https://doi.org/10.1007/s00604-013-1040-5
22. Abarca-Cabrera L, Fraga-García P, Berensmeier S (2021) Bio-nano interactions: binding proteins, polysaccharides, lipids and nucleic acids onto magnetic nanoparticles. Biomater Res 25:12. https://doi.org/10.1186/s40824-021-00212-y
23. Rojas-Sánchez L, Zhang E, Sokolova V, Zhong M, Yan H, Lu M, Li Q, Yan H, Epple M (2020) Genetic immunization against hepatitis B virus with calcium phosphate nanoparticles in vitro and in vivo. Acta Biomater 110:254–265. https://doi.org/10.1016/j.actbio.2020.04.021
24. Blanco E, Shen H, Ferrari M (2015) Principles of nanoparticle design for overcoming biological barriers to drug delivery. Nat Biotechnol 33:941–951. https://doi.org/10.1038/nbt.3330
25. Suk JS, Xu Q, Kim N, Hanes J, Ensign LM (2016) PEGylation as a strategy for improving nanoparticle-based drug and gene delivery. Adv Drug Deliv Rev 99:28–51. https://doi.org/10.1016/j.addr.2015.09.012
26. Nandhakumar S, Dhanaraju MD, Sundar VD, Heera B (2017) Influence of surface charge on the in vitro protein adsorption and cell cytotoxicity of paclitaxel loaded poly(ε-caprolactone) nanoparticles. Bull Fac Pharm Cairo Univ 55:249–258. https://doi.org/10.1016/j.bfopcu.2017.06.003
27. Boonchom B, Puttawong S (2010) Thermodynamics and kinetics of the dehydration reaction of $FePO_4{\cdot}2H_2O$. Physica B 405:2350–2355. https://doi.org/10.1016/j.physb.2010.02.046
28. Palacios E, Leret P, Fernández JF, De Aza AH, Rodríguez MA (2012) Synthesis of amorphous acid iron phosphate nanoparticles. J Nanopart Res 14:1131. https://doi.org/10.1007/s11051-012-1131-y
29. Huang F, Su Y, Long Z, Chen G, Yao Y (2018) Enhanced formation of 5-hydroxymethylfurfural from glucose using a silica-supported phosphate and iron phosphate heterogeneous catalyst. Ind Eng Chem Res 57:10198–10205. https://doi.org/10.1021/acs.iecr.8b01531
30. Stodt MFB, Gonchikzhapov M, Kasper T, Fritsching U, Kiefer J (2019) Chemistry of iron nitrate-based precursor solutions for spray-flame synthesis. Phys Chem Chem Phys 21:24793–24801. https://doi.org/10.1039/C9CP05007H
31. Vollmer N, Ayers R (2012) Decomposition combustion synthesis of calcium phosphate powders for bone tissue engineering. Int J Self-Propag High-Temp Synth 21:189–201. https://doi.org/10.3103/S1061386212040073
32. Drechsel H, Fiallo M, Garnier-Suillerot A, Matzanke BF, Schünemann V (2001) Spectroscopic studies on iron complexes of different anthracyclines in aprotic solvent systems. Inorg Chem 40:5324–5333. https://doi.org/10.1021/ic0002723
33. Jamieson GC, Fox JA, Poi M, Strickland SA (2016) Molecular and pharmacologic properties of the anticancer quinolone derivative vosaroxin: a new therapeutic agent for acute myeloid leukemia. Drugs 76:1245–1255. https://doi.org/10.1007/s40265-016-0614-z
34. Ichikawa Y, Ghanefar M, Bayeva M, Wu R, Khechaduri A, Prasad SVN, Mutharasan RK, Naik TJ, Ardehali H (2014) Cardiotoxicity of doxorubicin is mediated through mitochondrial iron accumulation. J Clin Investig 124:617–630. https://doi.org/10.1172/JCI72931
35. Qin Y, Guo T, Wang Z, Zhao Y (2021) The role of iron in doxorubicin-induced cardiotoxicity: recent advances and implication for drug delivery. J Mater Chem B 9:4793–4803. https://doi.org/10.1039/D1TB00551K
36. Gammella E, Maccarinelli F, Buratti P, Recalcati S, Cairo G (2014) The role of iron in anthracycline cardiotoxicity. Front Pharmacol 5:25. https://doi.org/10.3389/fphar.2014.00025
37. Hershko C, Link G, Tzahor M, Kaltwasser JP, Athias P, Grynberg A, Pinson A (1993) Anthracycline toxicity is potentiated by iron and inhibited by deferoxamine: Studies in rat heart cells in culture. J Lab Clin Med 122:245–251. https://doi.org/10.5555/uri:pii:002221439390070F
38. Hentze MW, Muckenthaler MU, Andrews NC (2004) Balancing acts: molecular control of mammalian iron metabolism. Cell 117:285–297. https://doi.org/10.1016/S0092-8674(04)00343-5
39. Wu D, Wang W, He X, Jiang M, Lai C, Hu X, Xi J, Wang M (2019) Biofabrication of nano copper oxide and its aptamer bioconjugate for delivery of mRNA 29b to lung cancer cells. Mater Sci Eng C Mater Biol Appl 97:827–832. https://doi.org/10.1016/j.msec.2018.12.009
40. Chen W, Glackin CA, Horwitz MA, Zink JI (2019) Nanomachines and other caps on mesoporous silica nanoparticles for drug delivery. Acc Chem Res 52:1531–1542. https://doi.org/10.1021/acs.accounts.9b00116
41. Friedman AD, Kim D, Liu R (2015) Highly stable aptamers selected from a 2′-fully modified fGmH RNA library for targeting biomaterials. Biomaterials 36:110–123. https://doi.org/10.1016/j.biomaterials.2014.08.046
42. Reyes-Reveles J, Sedaghat-Herati R, Gilley DR, Schaeffer AM, Ghosh KC, Greene TD, Gann HE, Dowler WA, Kramer S, Dean JM, Delong RK (2013) mPEG-PAMAM-G4 nucleic acid nanocomplexes: enhanced stability, RNase protection, and activity of splice switching oligomer and poly I: C RNA. Biomacromol 14:4108–4115. https://doi.org/10.1021/bm4012425
43. Jiang S, Eltoukhy AA, Love KT, Langer R, Anderson DG (2013) Lipidoid-coated iron oxide nanoparticles for efficient DNA and siRNA delivery. Nano Lett 13:1059–1064. https://doi.org/10.1021/nl304287a
44. Kumal RR, Abu-Laban M, Hamal P, Kruger B, Smith HT, Hayes DJ, Haber LH (2018) Near-infrared photothermal release of siRNA from the surface of colloidal gold–silver–gold core–shell–shell nanoparticles studied with second-harmonic generation. J Phys Chem C 122:19699–19704. https://doi.org/10.1021/acs.jpcc.8b06117
45. Johnson BJ, Melde BJ, Dinderman MA, Lin B (2012) Stabilization of RNA through absorption by functionalized mesoporous silicate nanospheres. PLoS ONE 7:e50356. https://doi.org/10.1371/journal.pone.0050356
46. Huslig G, Marchell N, Hoffman A, Park S, Choi S-O, DeLong RK (2019) Comparing the effects of physiologically-based metal oxide nanoparticles on ribonucleic acid and RAS/RBD-targeted triplex and aptamer interactions. Biochem Biophys Res Commun 517:43–48. https://doi.org/10.1016/j.bbrc.2019.06.164
47. Sokolova VV, Radtke I, Heumann R, Epple M (2006) Effective transfection of cells with multi-shell calcium phosphate-DNA nanoparticles. Biomaterials 27:3147–3153. https://doi.org/10.1016/j.biomaterials.2005.12.030
48. Rayamajhi S, Marchitto J, Nguyen TDT, Marasini R, Celia C, Aryal S (2020) pH-responsive cationic liposome for endosomal escape mediated drug delivery. Colloids Surf B 188:110804. https://doi.org/10.1016/j.colsurfb.2020.110804
49. Rayamajhi S, Nguyen TDT, Marasini R, Aryal S (2019) Macrophage-derived exosome-mimetic hybrid vesicles for tumor targeted drug delivery. Acta Biomater 94:482–494. https://doi.org/10.1016/j.actbio.2019.05.054
50. Rayamajhi S, Marasini R, Nguyen TDT, Plattner BL, Biller D, Aryal S (2020) Strategic reconstruction of macrophage-derived extracellular vesicles as a magnetic resonance imaging contrast agent. Biomater Sci. https://doi.org/10.1039/D0BM00128G
51. Nguyen TDT, Marasini R, Rayamajhi S, Aparicio C, Biller D, Aryal S (2020) Erythrocyte membrane concealed paramagnetic polymeric nanoparticle for contrast-enhanced magnetic resonance imaging. Nanoscale 12:4137–4149. https://doi.org/10.1039/D0NR00039F
52. DeLong RK, Dean J, Glaspell G, Jaberi-Douraki M, Ghosh K, Davis D, Monteiro-Riviere N, Chandran P, Nguyen T, Aryal S, Middaugh CR, Chan Park S, Choi S-O, Ramani M (2020) Amino/amido conjugates form to nanoscale cobalt physiometacomposite (PMC) materials functionally delivering nucleic acid therapeutic to nucleus enhancing anticancer activity via Ras-targeted protein interference. ACS Appl Biol Mater 3:175–179. https://doi.org/10.1021/acsabm.9b00798

Publisher's Note